New Journal of Physics
The open-access journal for physics

Picosecond temperature and pressure jumps in ice

Marcus Schmeisser, Andy Thaller, Hristo Iglev[1] and Alfred Laubereau

Physik-Department E11, Technische Universität München, D-85748 Garching, Germany
E-mail: higlev@ph.tum.de

New Journal of Physics **8** (2006) 104
Received 7 April 2006
Published 19 June 2006
Online at http://www.njp.org/
doi:10.1088/1367-2630/8/6/104

Abstract. A sensitive picosecond thermometer and manometer for hydrogen-bonded systems is demonstrated. The technique is applied for temperature jumps in ice by the help of subpicosecond pulses in the mid-infrared. The hydroxilic stretching vibrations (OH or OD) are applied for energy deposition and for the fast and sensitive spectral probing of local structure and thermodynamic condition. The method is verified in isotopically mixed ice at 200 K and ambient pressure. The transient data show that the local quasi-equilibrium in ice builds up within 25 ps allowing definition of a local temperature. Measurements performed close to the melting point provide no evidence for melting after energy deposition, but for substantial superheating of the ice lattice to 300 K that persists over the monitored time interval of 1.3 ns.

Contents

[1] Author to whom any correspondence should be addressed.

PII: S1367-2630(06)22193-1

1. Introduction

Because of its outstanding role in nature, the investigation of the physical properties of water has a long tradition in science. Many of these properties display an unusual temperature dependence that is attributed to the three-dimensional H-bonded network of water molecules [1]–[3], e.g. the density anomaly of the liquid. An important question in this context is the microscopic understanding of the ice–water phase transition. The structural changes in ice that undergoes the melting process are governed by the properties of the hydrogen-bonding network. On the molecular scale, the dynamics are connected with vibrational motions of the H-bonded groups, the breaking and reformation of H-bonds, and/or the displacement of hydrogen atoms. Such processes cover a multitude of timescales, with many elementary events occurring in the picosecond or even femtosecond time domain [4]–[6]. Consequently, the comprehension of the melting of ice requires investigations on an ultrashort timescale. But a basic problem here is to define a temperature and measure it properly on an ultrashort timescale.

We present ultrafast temperature jump measurements in an isotopically mixed ice containing 15 M HDO in D_2O (HDO : D_2O). The technique can be readily extended to other H-bonded systems [7]. The hydroxilic stretching vibrations (OH or OD) possess subpicosecond population lifetimes [8, 9] that allow a rapid energy deposition and redistribution. In order to define a temperature of the ice lattice and to measure it properly on an ultrashort timescale we have developed a sensitive picosecond thermometer [10]. The technique applies the OH and OD stretching vibrations, which are known as fast and sensitive probes for H-bonding [5, 11]. These vibrations represent suitable spectral tools to distinguish local structures with a time resolution of a few picoseconds [5, 6]. The use of the stretching modes as a picosecond thermometer of the local temperature of ice, monitoring the chemical equilibrium of the H-bonding network, is demonstrated in the following.

To illustrate this point, the common, steady-state infrared (IR) absorption spectrum of a crystalline mixture of HDO : D_2O (15 M), containing also negligible amounts of H_2O, is shown in figure 1 for various temperature values in the range from 170 (blue) to 270 K (red). The significantly different spectra of the molten sample at 275 K (black solid line), 280 K (dashed line) and 285 K (dash-dotted line) are depicted for comparison. In the range 2000–4000 cm^{-1}, the well-known OD- (left) and OH-bands (right) of ice display remarkable changes of shape and position (blueshift) with temperature. It is important to note here that the temperature effect on the absorption of the OH-stretching mode of the HDO : D_2O is nearly linear. The more complex shaping of the OD-band is because of the different temperature effect on the symmetric and anti-symmetric stretching vibrations of the D_2O bulk molecules.

Figure 2 presents the same data as thermal differential spectra for temperature differences 230–210 K (blue line), 250–230 K (green) and 270–250 K (red) respectively. The figure shows that for the OH mode, both amplitude and spectral shape of the thermal differential spectra depend only slightly on initial sample temperature. The differential spectrum corresponding to melting of the ice sample is also shown in figure 2 with the vertical scale reduced by a factor of five (black line). The potential of the molecular vibration as a local probe is readily seen from figures 1 and 2.

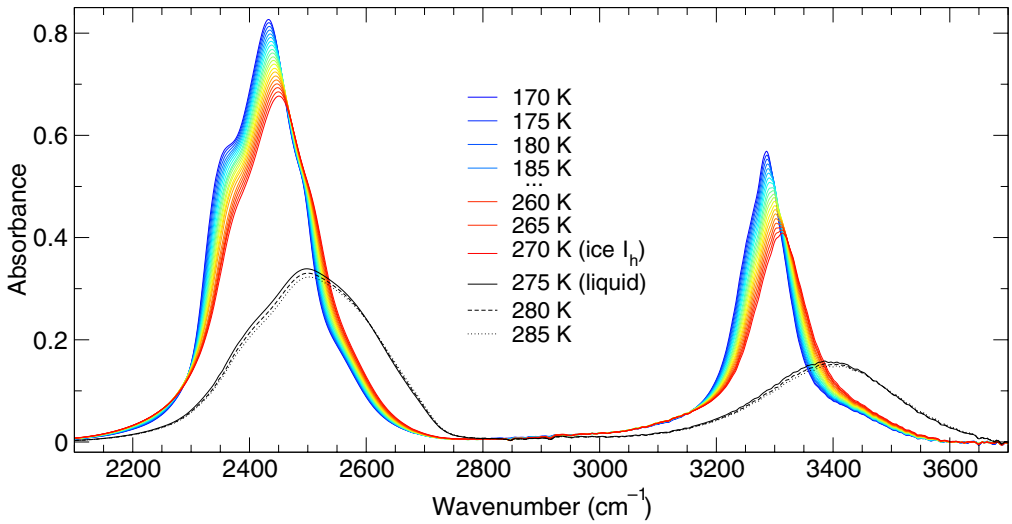

Figure 1. Conventional IR absorption spectra of HDO : D_2O (15 M) ice at various temperature values in the range from 170 (blue) to 270 K (red). The spectra of the molten sample at 275 K (black solid line), 280 K (dashed) and 285 K (dotted) are depicted for comparison. The drastic change of the IR absorption spectrum due to the ice–water phase transition should be noted.

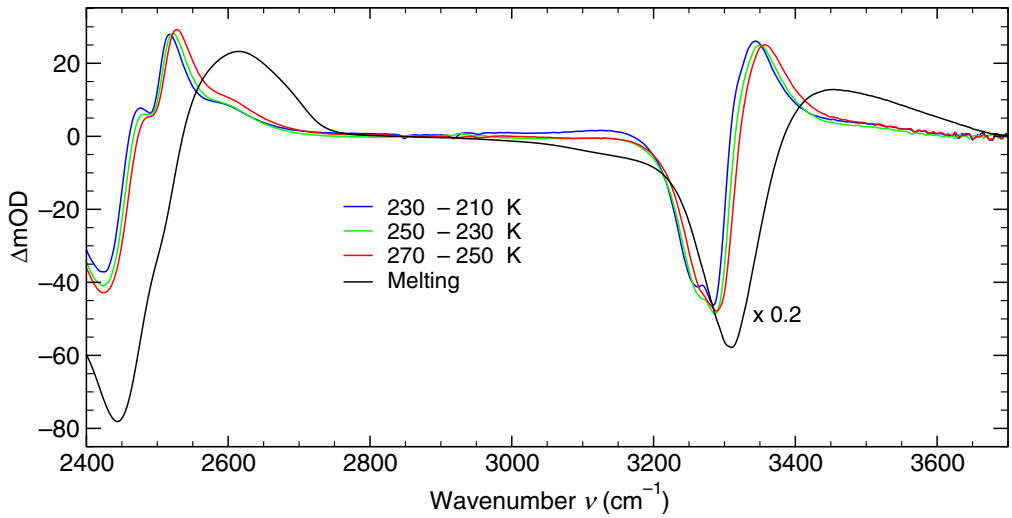

Figure 2. Same data as in figure 1 plotted as thermal differential spectra with $\Delta T = 20$ K for an initial sample temperature of 210 K (blue line), 230 K (green) and 250 K (red), respectively. For a better view, the spectrum corresponding to melting of the ice sample is scaled by a factor of 0.2 (275–270 K, black line).

2. Experimental setup

Our time-resolved measurements are performed using IR double-resonance spectroscopy. A schematic of the experimental system is shown in figure 3. We start with a Kerr-lens mode-locked Nd : YLF laser oscillator with a repetition rate of 43 Hz [12]. The laser emits long trains

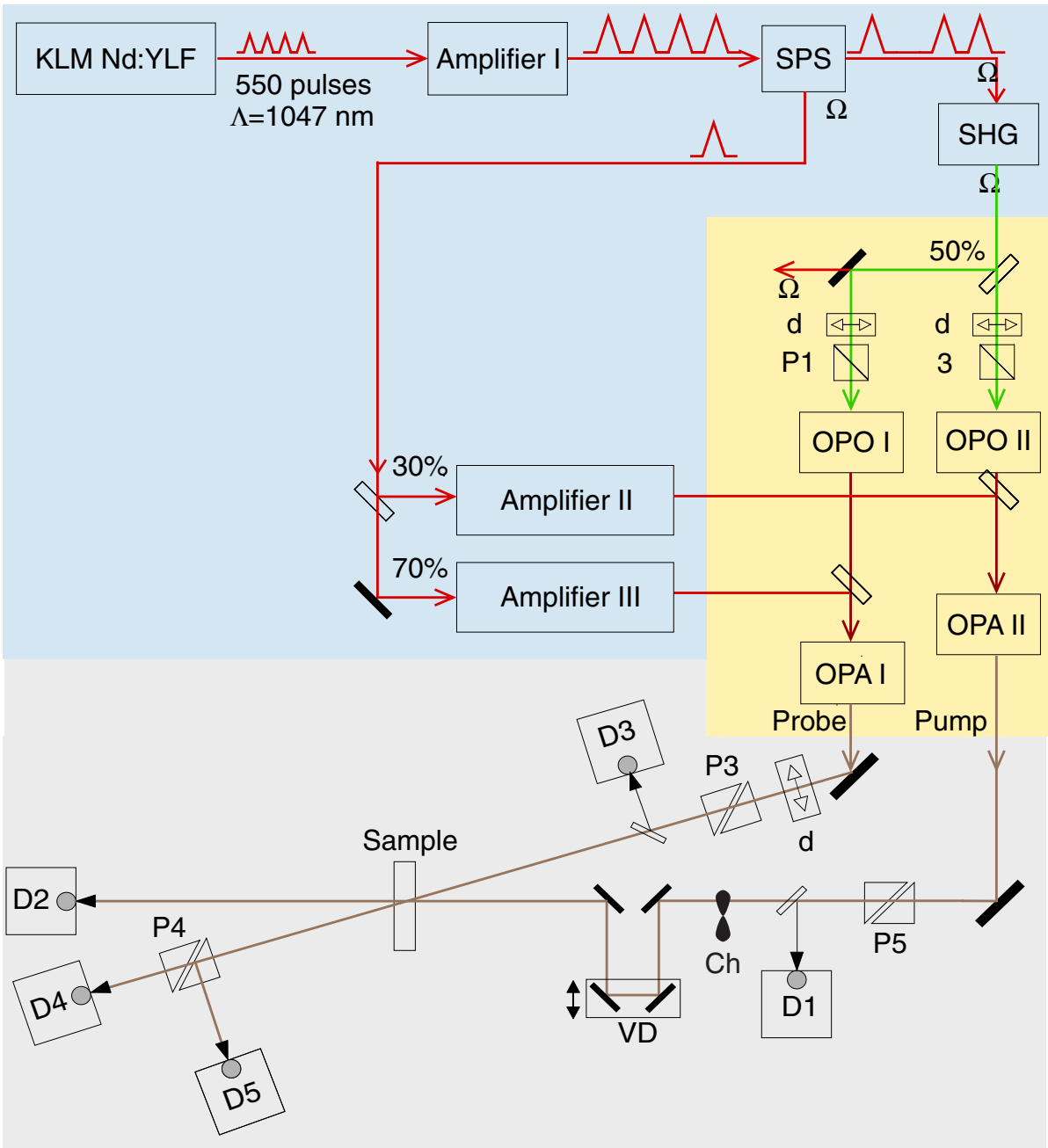

Figure 3. Schematic of the experimental setup for generation of two independently tunable mid-IR pulses with adjustable duration designed for two-colour pump–probe spectroscopy in the mid-IR; SPS, single-pulse selector; SHG, second harmonic generation; OPO, optical parametric amplifier; OPA, optical parametric amplifier; P1–P5, polarizers; $\lambda/2$, half-wave plates; VD, variable optical delay; Ch, chopper; D1–D5, mid-IR detectors.

lasting ≈5.5 μs of individual pulses with 10 ns separation, duration of 2.7 ps and energy of 1.2 μJ. Amplification of the pulse sequence followed by frequency doubling provides pulses at 523.5 nm of 3.5 ± 0.2 ps pulse duration and energy up to 7 μJ. The frequency-doubled laser radiation is used for synchronous pumping of two single-resonant optical parametric oscillators (OPO I and OPO II in figure 3). The idler components display pulse durations of 0.3–3 ps in the wavelength range 1.2–1.7 μm and single-pulse energy of approximately 10 nJ. The frequency tuning and the OPO pulse duration are computer controlled. The synchronization between the pulses of the two OPOs is better than 50 fs.

A single-pulse selector picks one pulse out of the amplified laser emission that is split into two parts with a ratio 30 : 70. Subsequent amplification yields two laser pulses with energies of 0.2 and 1 mJ, respectively, that serve as pump radiation for the two optical parametric amplifiers (OPA I and OPA II in figure 3). Parametric amplification of one selected pulse of the OPO in OPA I or OPA II is accompanied by the generation of the desired mid-IR difference-frequency component. In this way, two independent tunable IR pulses with duration of 0.7 ps (0.9 ps), spectral width of 24 cm^{-1} (19 cm^{-1}) and typical energy of 10 nJ (3 μJJ) are generated by two OPAs. Computer-controlled tuning is provided in the range 1700–3700 cm^{-1} (2300 to 3700 cm^{-1}). The numbers in brackets refer to the pump pulses. The diameter of the pump beam in the sample is approximately 150 μm and a factor of two larger than that of the probe. The delay time zero setting and the cross-correlation between the two IR-pulses are determined via two-photon absorption in a Ge specimen [13]. The energy transmittance $T(\nu)_{\parallel,\perp}$ of the probing pulse through the excited sample is measured for parallel ($\parallel$) and perpendicular ($\perp$) polarizations relative to the polarization plane of the pump pulse and compared with the probe transmittance $T_0(\nu)$ for blocked excitation beam. In this way, the induced absorption changes $\Delta OD_{\parallel,\perp}$ are determined for various probe frequencies ν and delay times t_D. The isotropic absorption signal, defined as $\Delta OD(\nu, t_D)_{iso} = -[\log(T/T_0)_{\parallel} + 2\log(T/T_0)_{\perp}]/3$ is determined and plotted in figures 4–11. We have verified experimentally that accumulative effects related to the repetition rate of the laser system are negligible.

The investigated samples consist of 15 M HDO in D_2O prepared by isotopic exchange in a mixture of appropriate amounts of D_2O (>99.9 atom %D) and tri-distilled H_2O. The ice crystals are grown by slowly cooling the isotopic mixture between two CaF_2 windows with 2.5 μm spacer in a cryostat to 180 K and warming it up to the desired temperature at ambient pressure later on.

3. Results and discussion

3.1. Ultrafast heating of HDO : D_2O (15 M) ice at an initial temperature of 200 K

The time evolution of the spectral changes induced after subpicosecond excitation at 2435 cm^{-1} (OD-pumping) and 3290 cm^{-1} (OH-pumping) of HDO : D_2O ice at 200 K are depicted as a contour plot in figures 4(a) and (b), respectively, with delay time plotted on the ordinate versus spectral position on the abscissa. We note here that the delay time is on a linear scale up to 10 ps, and on a logarithmic scale for longer delays. The change of the optical density of the sample is indicated by a colour code on the top of the figure with induced absorption in the blue and bleaching in the red. The pulse energies are adjusted to deposit approximately equal amounts of energy in both cases. It is interesting to note here that OH-pumping selects the minority species HDO, while OD-excitation mostly addresses D_2O bulk molecules.

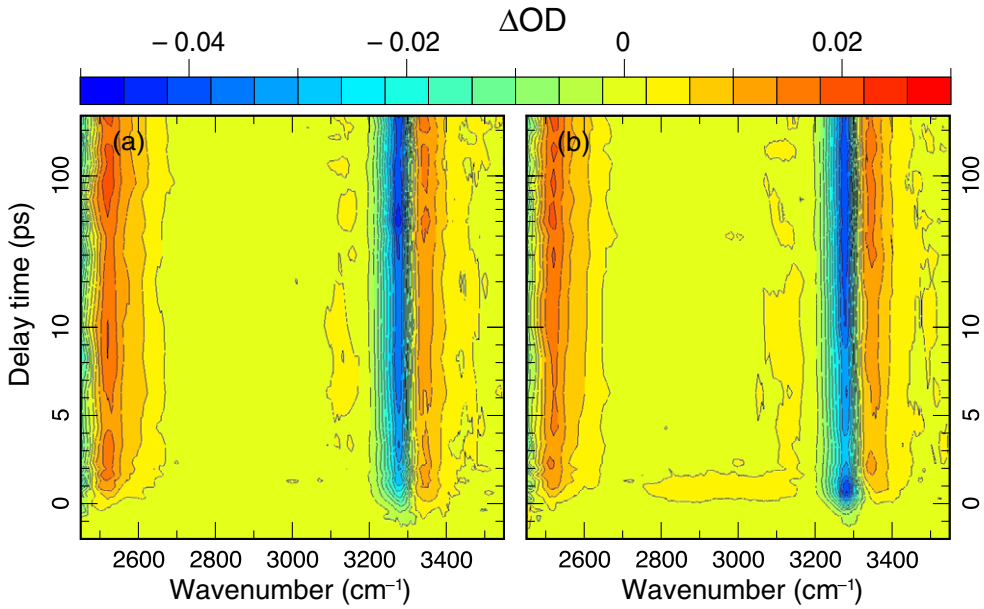

Figure 4. Time resolved data for HDO : D_2O ice at 200 K. Contour plot of the spectral changes induced by OD-pumping at 2435 cm^{-1} (a) and by OH-pumping at 3290 cm^{-1} (b) as a function of probe frequency and delay time. The changes of the optical density (ΔOD_{iso}) are indicated by contour values given in the colour scale on the top, with induced absorption in red and bleaching in blue. We note that the delay time is on a linear scale up to 10 ps, and on a logarithmic scale for longer delays.

Figures 4(a) and (b) show that the two excitation schemes induce very similar spectral changes, except the initial relaxation dynamics for $t_D < 3$ ps. The observation is consistent with the reported fast relaxation of the hydroxilic stretching vibrations in ice [5, 9]. The broad absorption in the range from 2750 to 3150 cm^{-1} detected after OH-pumping is assigned to the excited state absorption (ESA) of the initially excited OH-stretching mode. As expected for unharmonic oscillators [14] the ESA is red-shifted compared to the ground state absorption (see figure 1). The feature is not observed in figure 4(a) for OD-pumping because the ESA of the OD-mode is expected to occur for frequencies below 2400 cm^{-1}, i.e. beyond the monitored spectral range.

More quantitative data are displayed in figures 5 and 6 for fixed probe frequencies and delay times, respectively. The temporal evolution of the induced bleaching at 3280 cm^{-1} (blue points) and absorption at 2520 cm^{-1} (red points) is illustrated on figures 5(a), (b) and (c), (d), respectively, for both excitation conditions at 2435 cm^{-1} (filled diamonds in figures 5(a) and (c)) and 3290 cm^{-1} (open squares in figures 5(b) and (d)). For short delay times, the data indicate fast signal changes for both pumping schemes at rates comparable to our time resolution. The signal overshoot around $t_D = 0$ ps for similar pump and probe frequencies (see the insets of figures 5(b) and (c); the dashed line refers to the pump pulse duration) points towards a coherent pump–probe artifact in addition to vibrational population changes. This artifact is a well-known phenomenon for various materials, possibly due to cross-phase modulation or impulsive Raman scattering in the sample [15, 16]. It occurs for similar pump and probe frequencies, but not for notably different frequencies (see the insets of figures 5(a) and (d)).

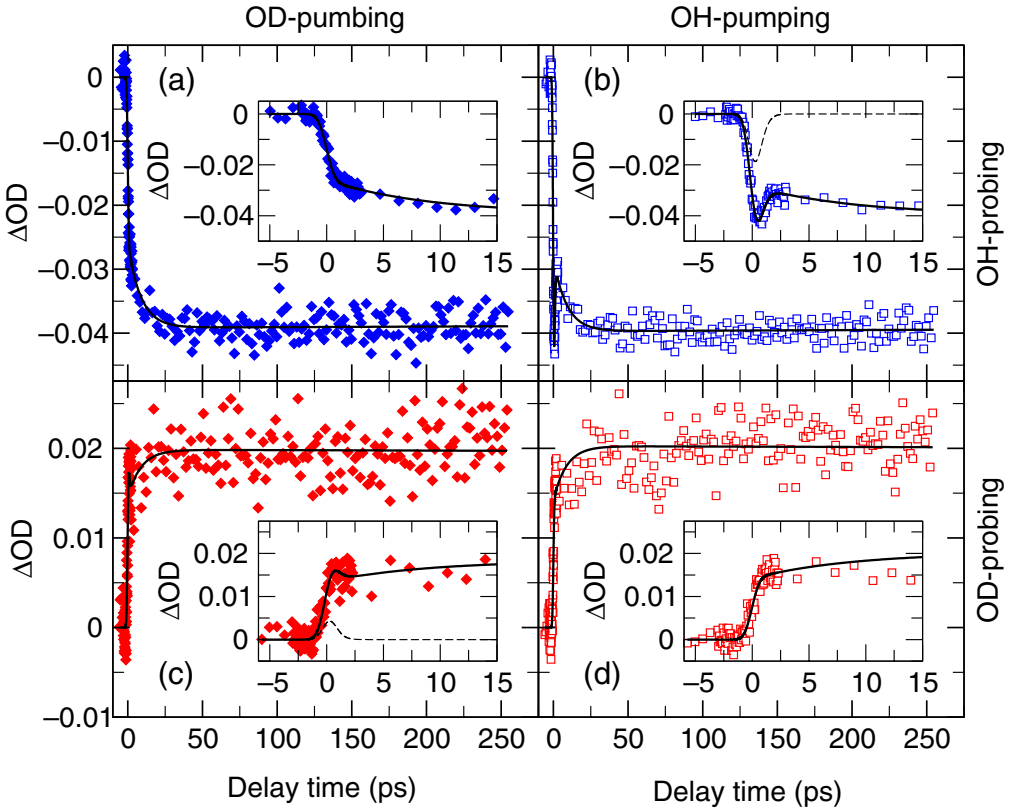

Figure 5. Temporal evolution of the induced bleaching in OH-mode at 3280 cm^{-1} (a and b) and absorption in OD-mode at 2520 cm^{-1} (c and d) measured in HDO : D_2O ice at initial temperature $T_i = 200$ K. Both, IR excitation at 2435 cm^{-1} (OD-pumping, a and c) and 3290 cm^{-1} (OH-pumping, b and c), is applied. A magnification of short delay times are presented in the inset of the corresponding figure, indicating fast signal changes for both pumping schemes at rates comparable to our time resolution. The dashed curves represent the contribution of a coherent pump–probe artifact and are mostly related to the pump pulse duration.

For delay times longer than 25 ps, an almost constant amplitude level is reached for all pump-probing conditions. The finding indicates an approximate local quasi-equilibrium at this time. The solid curves in figures 5(a)–(d) are calculated with the help of a simple two-step relaxation model involving exponential time constants τ_1 and τ_2. The short relaxation time $\tau_1 \leqslant 0.5$ ps derived from the data agree with the reported OH-lifetime of HDO : D_2O ice [8, 9]. The second time constant is measured to be $\tau_2 = 8.7 \pm 0.5$ ps and assigned to energy redistribution among low-frequency intermolecular vibrations, i.e. thermalization of the H-bonded network.

The transient differential spectra measured 40 ps after ultrafast heating of HDO ice at 200 K by OH- (3290 cm^{-1}, open squares) or OD-pumping (2435 cm^{-1}, filled diamond) respectively, are presented in figure 6. For better view, a magnification of the OD- and OH-region is shown in figures 6(a), (c) and (b), (d), respectively, where the same set of time-resolved data is displayed twice. The figures show that the two excitation schemes induce almost the same spectral changes.

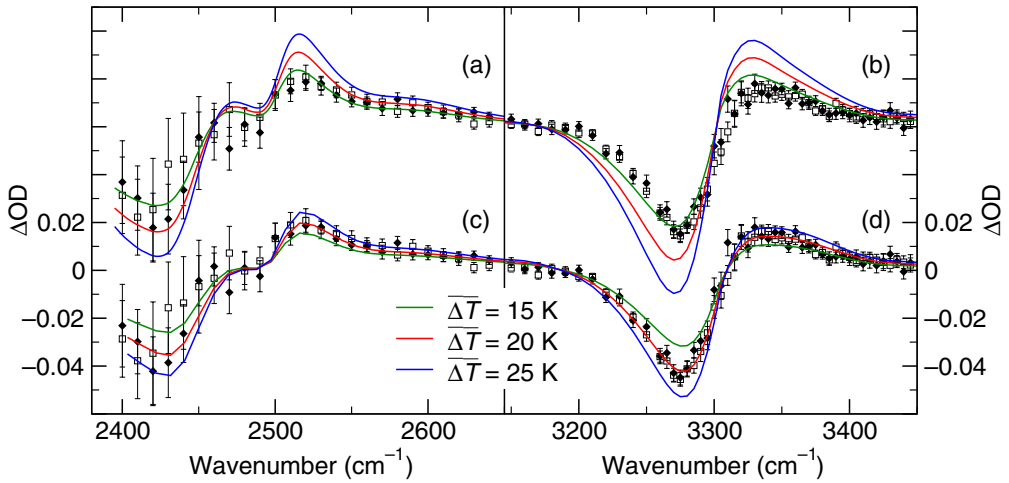

Figure 6. (a, b) Transient differential spectra measured with tunable sub-picosecond pulses 40 ps after OH- (open squares) or OD-pumping (filled diamond) of the HDO ice at 200 K. The curves represent steady-state thermal differential spectra for $\Delta T = 15$, 20 and 25 K and constant pressure. (c, d) Same picosecond data (experimental points) but compared to steady-state differential spectra for isochoric temperature jumps (calculated curves). The better agreement should be noted.

The finding obviously indicates that the OH- and OD-oscillators are in a local equilibrium at $t_D = 40$ ps.

Precise steady-state absorption data are measured using the same laser apparatus and the identical samples just blocking the pump beam. In this way, a convolution procedure required for conventional IR data (that were also available) with the spectral intensity distribution of our subpicosecond probe pulses was circumvented. The thermal differential spectra derived from steady-state data at constant pressure are presented in figures 6(a) and (b) for the temperature differences 215–200 K (green line), 220–200 K (red) and 225–200 K (blue). The similarity of these spectra with the time-resolved data verifies the expected heating of the ice sample by absorbing pump photons. In order to calibrate our picosecond thermometer, we have to take into account that the ultrafast temperature rise of the sample occurs at constant volume leading to a simultaneous pressure increase because of the slow volume expansion on a nanosecond timescale (see below), while conventional IR-data are taken at constant pressure. Raman studies on ice I_h under pressure [17, 18] reported a down-shift of -78 ± 7 cm^{-1} GPa^{-1} of the frequency of the OH-band. The OD-stretching mode is expected to display a corresponding shift approximately a factor $\sqrt{2}$ smaller.

Taking into account the coefficient of thermal volume expansion of ice, 155 MK^{-1} [19], and the isothermal compressibility of 120 MPa^{-1} [20], we derive the isochoric pressure increase of approximately 1.3 MPa K^{-1}. Using the pressure shifts of the hydroxilic Raman bands of HDO ice, we estimate the frequency shift of the isochoric thermal differential spectrum relative to the isobaric one by $-0.10 \pm .01$ cm^{-1} K^{-1} for the OH-mode and $-0.07 \pm .01$ cm^{-1} K^{-1} for the OD-mode, respectively. These numbers are used as correction factors for the evaluation of isochoric differential spectra from the measured isobaric steady state data, assuming that a moderate pressure jump does not change the spectral shape significantly.

The computed results for the thermal differential spectra for isochoric temperature jumps in the sample of 15 K (green line), 20 K (red) and 25 K (blue) are shown for the OD- and OH-band in figures 6(c) and (d), respectively. The data illustrate the sensitivity of the hydroxilic stretching vibrations on the local pressure and temperature. The good agreement of the red line with the transient data (especially for the OH-mode) is noteworthy, indicating an average temperature rise of the probed sample volume of $\overline{\Delta T} = 20 \pm 2$ K. The estimated average value for the simultaneous pressure increase at $t_D = 40$ ps is $\overline{\Delta P} = 26 \pm 5$ MPa in the probed sample volume. The considerably improved agreement between transient and stationary results in figures 6(c) and (d) relative to (a) and (b), respectively, gives experimental support to the isochoric character of the picosecond temperature jump of the sample.

For a strongly absorbing sample, as investigated here, it is important to consider the dissipation of excitation energy along the propagation direction z. Since the population changes generated by the pump pulse are negligible (linear absorption), the longitudinal energy profile in the probed sample volume is simply governed by Beer's law, $E(z) = E_0 \times 10^{-zA/d}$. Here, A is the sample absorbance at the pump frequency, E_0 represents the input energy of the pump pulse over the cross-section of the probing beam, and d denotes the sample thickness. The lateral energy profile is approximately constant because of the notably thicker pump beam in the sample. Neglecting also thermal conductivity on the macroscopic length scale (see below), the temperature rise induced in the sample varies with propagation length

$$\Delta T(z) = \frac{A \times \ln 10}{1 - 10^{-A}} \times \overline{\Delta T} \times 10^{-Az/d}.$$

Here $\overline{\Delta T}$ denotes the average temperature rise of the probed sample volume.

Analysing the transient differential spectra in terms of thermal (stationary) differential spectra, we are able to extract the slow changes of average temperature and pressure in the probed sample volume. To this end, the effects of temperature and pressure on the vibrational bands are treated separately in the fitting procedure. It is recalled that the pressure change is deduced from a band shift as compared to the isobaric spectrum. The results are summarized in figure 7 (experimental points), where the temporal evolutions of average temperature and pressure in the probed sample volume are presented. Our analysis shows that the hydrogen bonding network in the ice sample reaches a local quasi-equilibrium for $t_D > 25$ ps, which allows definition of a temperature value. Earlier experimental points in figure 7 are not meaningful and are displayed just for comparison. The stated experimental accuracy does not include a potential systematic error of the pressure scale that relies on the pressure coefficient of the OH- or OD-band position. It is gratifying to see the declining of temperature and pressure on the timescale of 10^{-10} s. Assuming an exponential decay, the time constant for the heat dissipation is estimated to be 2.5 ± 1 ns (red solid line in figure 7), consistent with estimations of the heat conduction to the cell windows. The pressure drops somewhat faster with $\approx$1 ns (0.5 to 2 ns). The phenomenon is dominantly assigned to adiabatic volume expansion. In fact, the propagation time of longitudinal/transverse acoustic waves through the thin ice specimen is estimated to be 0.6/1.3 ns (longitudinal/transverse sound velocity of 3.9/2.0 km s^{-1} [21, 22]). The nice agreement supports the reliability of this spectroscopic technique and demonstrates its potential as a remote picosecond thermometer and manometer.

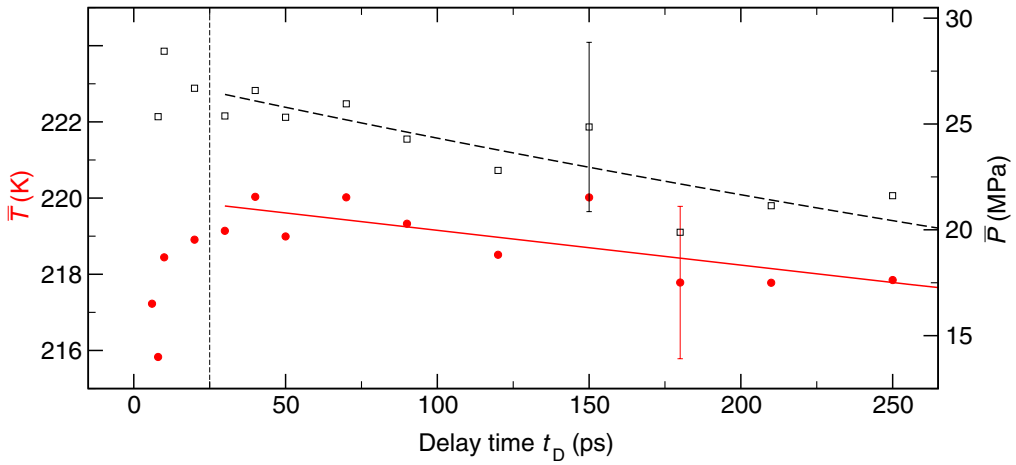

Figure 7. Average transient temperature and pressure of the probed sample volume following the ultrafast heating of the ice sample from 200 K at atmospheric pressure. The initial temperature jump (red filled circles, red solid line, left ordinate scale) to a quasi-equilibrium after ≈25 ps (vertical line) is consistent with an isochoric transition. Temperature and pressure (black open squares, black dashed line, right ordinate scale) develop differently later on.

3.2. Ultrafast superheating of HDO : D_2O ice at 270 K

Of particular interest are the experiments close to the melting point of the ice sample (T_m = 274.8 K) where the temperature rise may interfere with a melting process. The time-resolved data for an initial temperature of 270 K are presented in figure 8, while the other experimental conditions are the same as for 200 K (a minor adjustment of pump frequencies is required to match the shifted band maxima). Contour plots of the spectral changes induced by OD-pumping at 2450 cm^{-1} and OH-pumping at 3310 cm^{-1} are shown in figures 8(a) and (b) respectively, with delay time plotted on the ordinate versus spectral position on the abscissa. Note the linear ordinate scale below 10 ps and the logarithmic scale above this value. The striking similarity to the data of figure 4 should be noted, i.e. thermal blueshifts of the hydroxilic bands are found, but no significant broadening as required for the appearance of water. In other words, there is no evidence for (partial) melting within 250 ps.

The temporal evolution of the induced bleaching at 3300 cm^{-1} (blue points) and absorption at 2535 cm^{-1} (red points) are presented in figures 9(a), (b) and (c), (d), respectively, for OD-pumping (filled diamonds, figures 9(a) and (c)) and OH-pumping (open squares, figures 9(b) and (d)). The insets present the early absorption changes with stretched delay timescales. Again, only evidence for a temperature rise is found. The thermalization of the ice lattice occurs somewhat faster than at 200 K. The new quasi-equilibrium, as indicated by the induced absorption changes, has established within 15 ps. In fact, fitting the two-stage relaxation model to the data, mentioned above in context with figure 5, yields the thermalization time $\tau_2 = 5.4 \pm 0.5$ ps (and $\tau_1 \leqslant 0.5$ ps).

Examples for the time evolution of the differential spectra of HDO ice at 270 K after OH-pumping at 3310 cm^{-1} are shown in figure 10, measured at various delay time values from 10 ps to 1.33 ns (experimental points, calculated solid curves). For shorter delay times a modification of the spectral profile is noticed that is assigned to the thermalization process, e.g. the redistribution

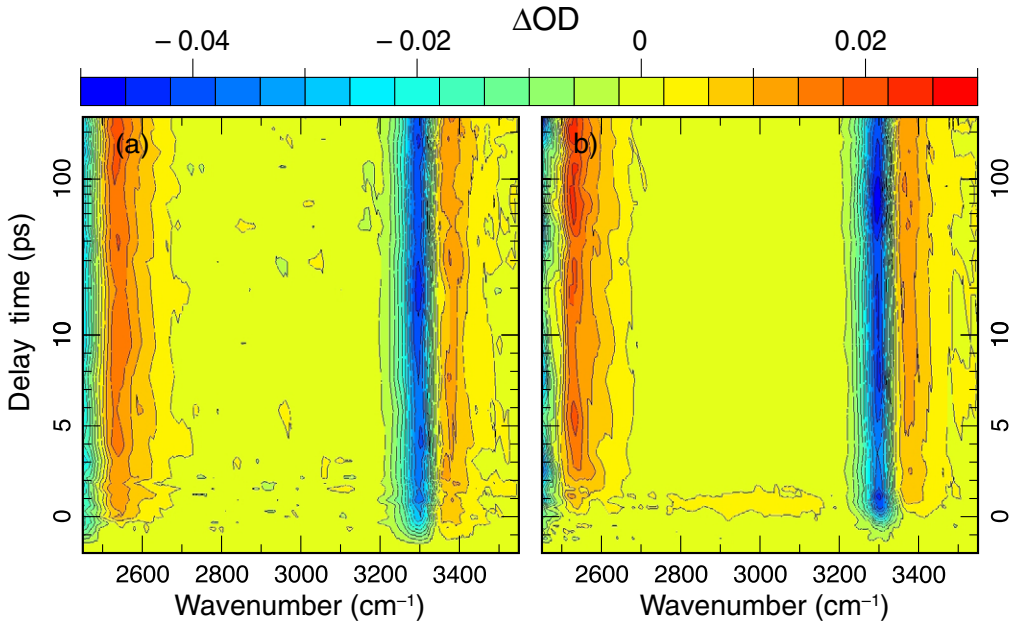

Figure 8. Same as figure 4 but for an initial temperature of 270 K. Contour plot of the spectral changes induced by OD-pumping at 2450 cm^{-1} (a) and by OH-pumping at 3310 cm^{-1} (b) as a function of probe frequency and delay time. We note that the delay time is on a linear scale to 10 ps, and on a logarithmic scale for longer delays. The striking similarity to the data on figure 4 should be noted.

of the energy among low-frequency intermolecular vibration. For longer delay times ($\geqslant$25 ps), the data show a nearly constant amplitude level and shape of the differential spectra. The blue dashed line in the figure represents the calculated steady-state differential spectrum assuming that the probed volume is heated from 270 to 274.8 K with subsequent melting of 10% of the ice sample. Most important, this curve notably differs from the experimental data and demonstrates the sensitivity of the measurements to a phase transition.

As suggested by the similarity of the signals measured at both temperatures, it is straightforward to assume that the optical excitation induces the same process. To verify this point, we numerically generate thermal differential spectra of HDO : D_2O ice for temperature values above the melting point by extrapolation of the temperature dependence of the steady-state spectra. The measured conventional IR spectra in the range 200–270 K show that both amplitude and spectral shape of the thermal differential spectra depend only slightly on the initial temperature, while the spectral position is shifted by $(\Delta\nu_{OH}/\Delta T)_P = 0.41 \pm 0.02\,cm^{-1}\,K^{-1}$ at 270 K (see figure 2). Accordingly, we define a hypothetical stationary differential spectrum beyond the melting point by an extrapolation of this dependence, including also the isochoric pressure increase with its corresponding band shifts. The results of the simulation for different isochoric temperature jumps are indicated by the solid curves in figure 10. The lines nicely reproduce the experimental data suggesting an averaged temperature rise of 20 K in the sample.

The averaged temperature and pressure in the probed sample volume extracted from the measured band-shape changes (compare black solid curves in figure 10) are summarized in figure 11 and show nearly the same time evolution as at 200 K. An average temperature in the

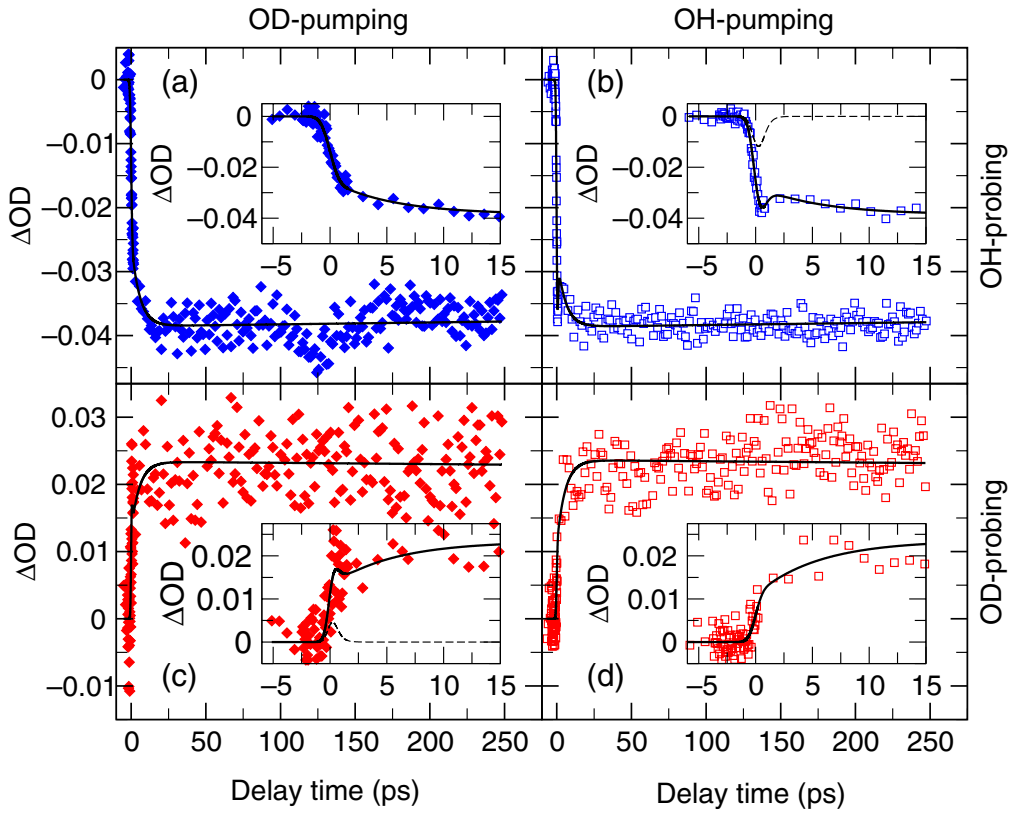

Figure 9. Time evolution of the induced bleaching at 3300 cm^{-1} (a and b) and absorption at 2535 cm^{-1} (c and d) measured in HDO : D_2O ice at 270 K, after excitation at 2450 cm^{-1} (OD-pumping, a and c) and 3310 cm^{-1} (OH-pumping, b and c). The dashed curves represent the contribution of the coherent pump–probe artifact.

DHO:D_2O ice sample up to 290 K is observed. Figure 10 shows that the superheated ice state persists more than 1.33 ns. The absence of melting of our sample within 1.33 ns is noteworthy and cannot be explained by experimental shortcomings, since evidence for the phase transition was obtained at higher excitation levels [10]. According to the variation of the induced temperature rise along the propagation direction in the sample mentioned above, we estimate a superheating up to 300 K close to the front face of the ice specimen. The number is consistent with recent theoretical studies of ice where a possible superheating of 40 K [23] if not 70 K [24] was predicted. Superheating was previously reported for several other materials after ultrafast laser heating, but not yet for an H-bonded molecular crystal like ice [25, 26].

4. Conclusion

In conclusion, we have demonstrated a spectroscopic method for both temperature and pressure measurements in an H-bonded material on a picosecond timescale. The method is verified for an isotopic mixture of ice at 200 K and ambient pressure. We show that the use of a temperature scale is meaningful for ice as early as 25 ps after energy deposition. Using an ultrafast temperature

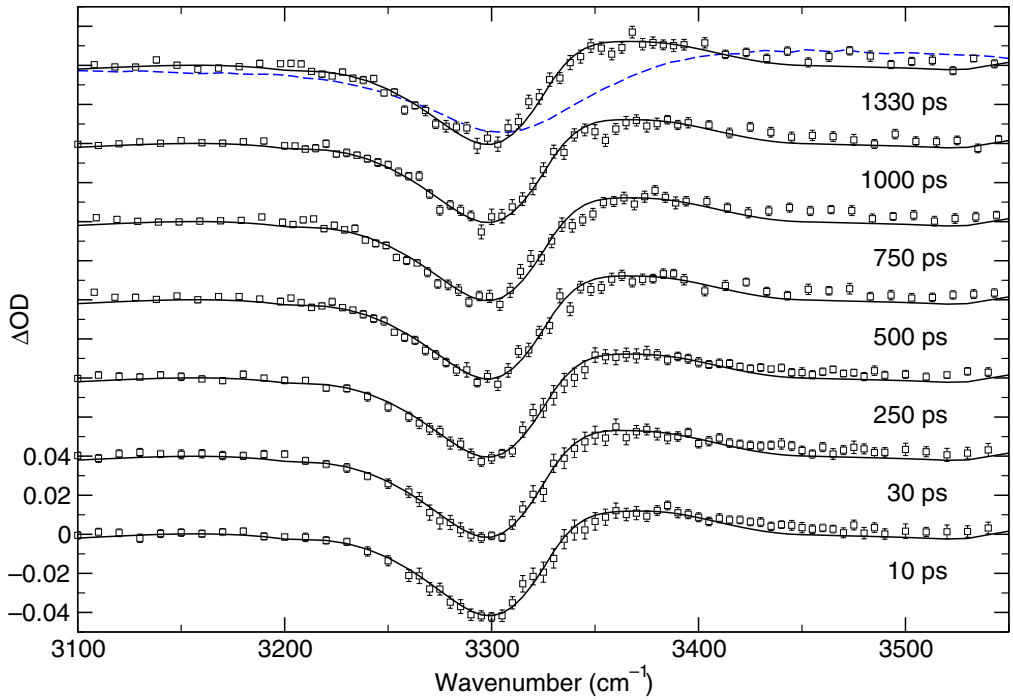

Figure 10. Time-resolved absorption spectra of HDO ice at 270 K at various delay time values after OH-pumping at 3310 cm^{-1} (experimental points). The spectra are vertically shifted by multiples of 0.04 OD. The black lines are calculated and represent extrapolated thermal differential spectra for isochoric temperature jump with transient temperature and pressure from figure 11. The blue dashed line refers to partial melting that cannot account for the observed spectral changes.

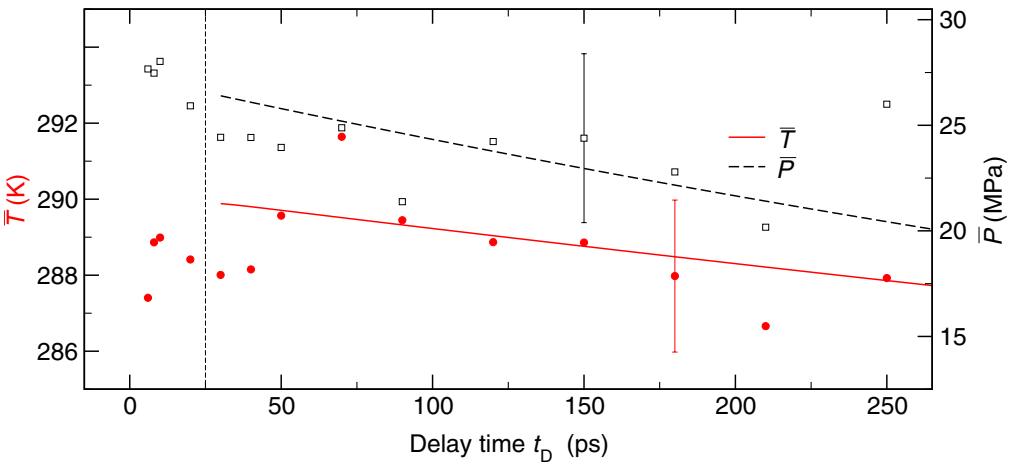

Figure 11. Average transient temperature and pressure of the probed sample volume following the ultrafast heating of the ice sample from 270 K at atmospheric pressure. The initial temperature jump (filled circles, solid line, left ordinate scale) to a quasi-equilibrium after ≈25 ps (vertical line) is consistent with an isochoric transition. Temperature and pressure (open squares, solid line, right ordinate scale) develop differently later on.

jump technique, we observe a heating of the HDO : D_2O ice up to 300 K that persists beyond 1.33 ns. The generated superheating of ice seems to be favoured on the one hand by the deposition of excitation energy in the bulk followed by rapid equilibration including intermolecular energy transport with a time constant below 10 ps. On the other hand, the thermal stability of the hydrogen bonds in the crystal lattice near the melting point appears to be higher as assumed at present.

References

[1] Nibbering E T J and Elsaesser T 2004 *Chem. Rev.* **103** 1887
[2] Chen B, Ivanov I, Klein M L and Parrinello M 2003 *Phys. Rev. Lett.* **91** 5503
[3] Petrenko V F and Whitworth R W 2005 *Physics of Ice* (Oxford: Oxford University Press)
[4] Brena B *et al* 2005 *Phys. Rev. Lett.* **93** 148302
[5] Laenen R, Rauscher C and Laubereau A 1998 *Phys. Rev. Lett.* **80** 2622
[6] Woutersen S, Emmerichs U and Bakker H 1997 *Science* **278** 658
[7] Austin R H *et al* 2005 *Phys. Rev. Lett.* **94** 128101
[8] Laenen R, Simeonidis K and Laubereau A 1999 *Laser Phys.* **9** 234
[9] Woutersen S, Emmerichs U, Nienhuys H and Bakker H 1998 *Phys. Rev. Lett.* **81** 1106
[10] Iglev H, Schmeisser M, Simeonidis K, Thaller A and Laubereau A 2006 *Nature* **439** 183
[11] Graener H, Seifert G and Laubereau A 1991 *Phys. Rev. Lett.* **66** 2092
[12] Lindenberger F, Stöckl R, Laenen R and Laubereau A 1995 *Opt. Commun.* **117** 268
[13] Laenen R, Simeonidis K and Laubereau A 1998 *J. Opt. Soc. Am.* B **15** 1213
[14] Huse N *et al* 2005 *Phys. Rev. Lett.* **95** 147402
[15] Kovalenko S A, Ruthmann J and Ernsting N P 1998 *J. Chem. Phys.* **109** 1894
[16] Ekvall K, van der Meulen P, Dhollande C, Berg L-E, Pommeret S, Naskrecki R and Mialocq J-C 2000 *J. Appl. Phys.* **87** 2340
[17] Minceva-Sukarova B, Sherman W F and Wilkinson G R 1984 *J. Phys. C: Solid State Phys.* **17** 5833
[18] Sivakumar T C, Chew H A M and Johari G P 1978 *Nature* **275** 524
[19] LaPlaca S and Post B 1960 *Acta Crystallogr.* **13** 503
[20] Gow A J and Williamson T C 1972 *J. Geophys. Res.* **77** 6348
[21] Gagnon R E, Kiefte H, Clouter M J and Whalley E 1988 *J. Chem. Phys.* **89** 4522
[22] Gagnon R E, Kiefte H and Clouter M J 1990 *J. Chem. Phys.* **92** 1909
[23] Luo S N, Strachan A and Swift D C 2005 *Modelling Simul. Mater. Sci. Eng.* **13** 321
[24] McBride C, Vega C, Sanz E, MacDowell L and Abascal J 2005 *Mol. Phys.* **103** 1
[25] Huang K C, Wang T and Joannopoulos J D 2005 *Phys. Rev. Lett.* **94** 175702
[26] Luo S N and Ahrens T J 2003 *Phys. Rev.* B **68** 134206